# Terahertz Ratchet Effect in Interdigitated HgTe Structures

I. Yahniuk,[1,2] G. V. Budkin,[3] A. Kazakov,[4] M. Otteneder,[1] J. Ziegler,[1] D. Weiss,[1] N. N. Mikhailov,[5]
S. A. Dvoretskii,[5] T. Wojciechowski,[4] V. V. Bel'kov,[3] W. Knap,[2,6] and S. D. Ganichev[1,2,*]

[1]*Terahertz Center, University of Regensburg, Regensburg D-93053, Germany*
[2]*Center for Terahertz Research and Applications (CENTERA), Institute of High Pressure Physics PAS,
Warsaw 01-142, Poland*
[3]*Ioffe Institute, St. Petersburg 194021, Russia*
[4]*International Research Centre MagTop, Institute of Physics, Polish Academy of Sciences, al. Lotników 32/46,
Warsaw PL02-668, Poland*
[5]*Institute of Semiconductor Physics, Siberian Branch, Russian Academy of Sciences, pr. Akademika Lavrent'eva
13, Novosibirsk 630090, Russia*
[6]*Laboratoire Charles Coulomb, Université de Montpellier, Centre National de la Recherche Scientifique,
Montpellier 34095, France*

The emergence of ratchet effects in two-dimensional materials is strongly correlated with the introduction of asymmetry into the system. In general, dual-grating-gate structures forming lateral asymmetric superlattices provide a suitable platform for studying this phenomenon. Here, we report on the observation of ratchet effects in HgTe-based dual-grating-gate structures hosting different band-structure properties. Applying polarized terahertz laser radiation we detect linear and polarization-independent ratchets, as well as a radiation-helicity-driven circular ratchet effect. Studying the ratchet effect in devices made of quantum wells (QWs) of different thickness, we observe that the magnitude of the signal substantially increases with decreasing QW width with a maximum value for devices made of QWs of critical thickness hosting Dirac fermions. Furthermore, sweeping the gate voltage amplitude we observe sign-alternating oscillations for gate voltages corresponding to $p$-type conductivity. The amplitude of the oscillations is more than two orders of magnitude larger than the signal for $n$-type conducting QWs. The oscillations and the signal enhancement is shown to be caused by the complex valence band structure of HgTe-based QWs. These peculiar features of the ratchet currents make these materials an ideal platform for the development of terahertz applications.

## I. INTRODUCTION

Mercury cadmium telluride based heterostructures belong to the most widely used materials for sensitive and fast infrared or terahertz detectors [1–9] and are among the most promising materials to realize high-quality topological insulators (TIs) [10–12]. The reason for this is the wide tunability of the energy spectrum of these materials, including the possibility of realizing an inverted band structure in HgTe-based structures. The latter is a crucial condition for the formation of helical edge and surface states [10–12]. This is also supported by the well-developed technological processes originally motivated by the fabrication of infrared radiation detectors, which has been adapted for the growth of high-quality TI materials. This includes the possibility to obtain high carrier

mobility while at the same time contributions from three-dimensional carriers in the bulk can be largely suppressed [5,13–17]. Thus, HgTe systems allow one to combine the excellent performance of HgTe-based infrared and terahertz sensors and advantages of topological systems, in particular, obtaining photon helicity sensitive photoresponses [17,18]. In the last decade, it has been demonstrated that ratchet effects in two-dimensional (2D) electron systems with lateral superlattices can be used for efficient detection of terahertz radiation and may even provide new functionalities, such as all-electric detection of the radiation Stokes parameters operating up to room temperature [19]. The ratchet effect, demonstrating strong photoresponses and considered as a candidate for efficient detection of terahertz radiation, has been observed and investigated in various 2D semiconductor structures with parabolic energy dispersion [20–31] and in monolayer graphene [32], but so far has not been detected in HgTe-based systems. Such a study, however, allows us to

---

*Corresponding author: sergey.ganichev@physik.uni-regensburg.de

combine advantages of the ratchet effect and the superior properties of HgTe-based materials for the infrared and terahertz radiation detection, as well as exploring the physical properties of HgTe-based QWs.

Here we report on the observation and study of polarization-dependent ratchet effects in HgTe-based quantum wells of different width. The effect is studied in QWs with a superimposed dual-grating gate (DGG), lateral asymmetric superlattices excited by normally incident terahertz laser radiation. The magnitude and direction of the ratchet current is shown to be dependent both on the polarization state of the radiation and on the lateral asymmetry determined by the gate voltages applied to the two subgates. By varying the radiation polarization we observe that the terahertz ratchet effect has three current contributions: polarization-insensitive, linear, and circular ratchet contributions. While the second one can be excited by linearly polarized radiation and is sensitive to the relative orientation of the electric field vector and the source-drain direction, the third one is driven by the radiation helicity and has opposite signs for right- and left-handed circularly polarized radiation. Measurements of the ratchet currents in HgTe QWs of different thickness allow us to study ratchet effects in HgTe-based QWs featuring different band-structure properties. Notably, the highest helicity-driven ratchet current is detected in a system with Dirac fermions. Studying the gate voltage dependence of the ratchet effect we, unexpectedly, observed the emergence of sign-alternating oscillations of the photoresponse at high negative gate voltages corresponding to $p$-type conductance. Our theoretical analysis demonstrates that the oscillations are caused by shifting the Fermi energy across the well-separated multiple valence subbands, which in turn results in oscillations of the density of states. The developed theoretical model, which takes into account the Seebeck ratchet mechanism and considers tiny details of the energy dispersion, describes the experimental results well.

## A. Experimental technique

Our devices are made of HgTe/(Hg,Cd)Te quantum well (QW) structures grown by molecular beam epitaxy on (013)-oriented GaAs substrates. The heterostructure

parameters such as QW thickness ($d_{\mathrm{QW}}$) and barrier composition are presented in Table I. The asymmetric inter-digitated DGG structures are fabricated by electron-beam lithography. Wet Br-based etching is used to define the channel geometries, having a channel length ranging from 50 to 75 $\mu$m and a channel width between 7 and 31 $\mu$m. Plasma-enhanced chemical vapor deposition is used to deposit 140-nm Si(ON) insulation, separating the HgTe/(Cd, Hg)Te heterostructure and the finger gates made of Ti (5 nm) and Au (100 nm). The full description of the growth, characterization and device preparation can be found in Refs. [33,34]. Figures 1(a) and 1(b) show an optical image of one of the DGG structures and a schematic illustration of the cross section of the device. The grating consists of periodically repeating asymmetric supercells that are separated by spacings $a_1$ and $a_2$. The asymmetry of the DGG structure stemming from the inequality of stripe widths ($d_1 < d_2$) and stripe separations ($a_1 < a_2$) is crucial for the generation of the ratchet effect. Below we denote the direction perpendicular to the metal fingers as the $x$ direction.

All thin stripes are connected by a metal film forming the gate G1, and all interconnected wide stripes form the gate G2. This allows us to create an asymmetric periodic electrostatic potential acting on the 2DEG by applying different voltages to the subgates G1 ($V_{\mathrm{G1}}$) and G2 ($V_{\mathrm{G2}}$). Table I presents the geometrical parameters of the DGG and period of the superlattice, $d = d_1 + a_1 + d_2 + a_2$. Ohmic contacts to source, drain, and gates are fabricated by In soldering. To characterize the structures, we perform transport and magnetotransport measurements. To measure the electrical resistance $R_{\mathrm{SD}}$, we use SR830 lock-in amplifiers with a low modulation frequency (13 Hz) and 0.1-$\mu$A current amplitude. All transport studies are carried out at $T = 4.2$ K. The source-drain resistance as a function of the gate voltage exhibits a clear maximum at negative values of the gate voltages $V_{\mathrm{G1}}$ or $V_{\mathrm{G2}}$. This demonstrates that besides the controllable modification of the lateral asymmetry, sweeping the gate voltage allows us to change the type of conductivity beneath the gates. The variation of the carrier density of the 2DEG in the HgTe QWs from $n$- to $p$-type occurs for a Fermi energy position in the insulating band gap. In this case, the resistance $R_{\mathrm{SD}}$ shows a maximum that corresponds to a change of the sign

TABLE I. Basic parameters of the structures investigated.

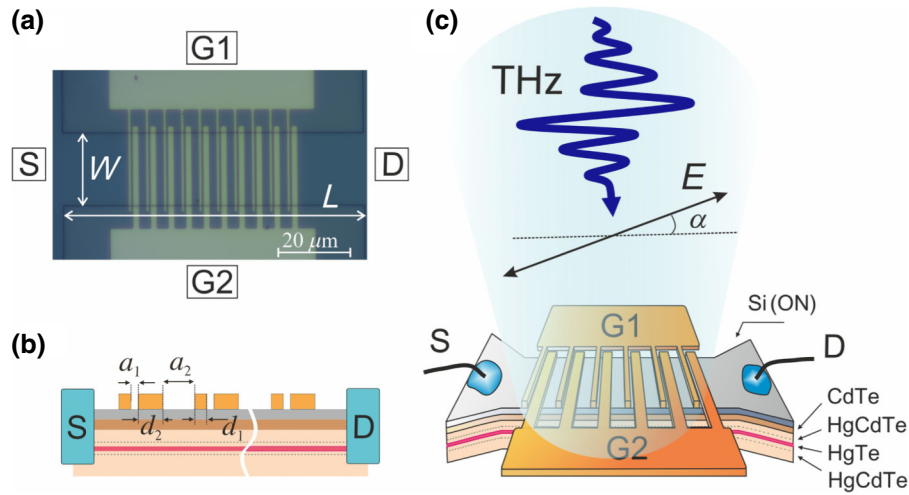| Devices | $d_{\mathrm{QW}}$ (nm) | Barrier composition | $L \times W$ ($\mu$m$^2$) | $d_1$ ($\mu$m) | $d_2$ ($\mu$m) | $a_1$ ($\mu$m) | $a_2$ ($\mu$m) | $d$ ($\mu$m) |
|---|---|---|---|---|---|---|---|---|
| D1 | 8.0 | $\mathrm{Hg_{0.23}Cd_{0.77}Te}$ | $72 \times 31$ | 0.75 | 2.25 | 1.0 | 3.5 | 7.5 |
| D2 | 7.0 | $\mathrm{Hg_{0.28}Cd_{0.72}Te}$ | $85 \times 20$ | 0.5 | 1.5 | 0.5 | 2.5 | 5.0 |
| D3 | 6.3 | $\mathrm{Hg_{0.42}Cd_{0.58}Te}$ | $50 \times 19$ | 0.5 | 1.5 | 0.5 | 2.5 | 5.0 |
| D4 | 7.0 | $\mathrm{Hg_{0.28}Cd_{0.72}Te}$ | $75 \times 15$ | 1.25 | 3.0 | 0.75 | 3.0 | 8.0 |
| D5 | 8.0 | $\mathrm{Hg_{0.23}Cd_{0.77}Te}$ | $75 \times 15$ | 1.25 | 3.0 | 0.75 | 3.0 | 8.0 |
| D6 | 8.0 | $\mathrm{Hg_{0.23}Cd_{0.77}Te}$ | $50 \times 7$ | 0.75 | 2.0 | 0.5 | 2.0 | 5.25 |
| D7 | 7.0 | $\mathrm{Hg_{0.28}Cd_{0.72}Te}$ | $72 \times 31$ | 0.75 | 2.25 | 1.0 | 3.5 | 7.5 |

FIG. 1.   (a) Picture of the interdigitated gate electrodes deposited on the HgTe/(Hg,Cd)Te heterostructure. All devices have four terminals: source (S), two gates (G1, G2), and drain (D). (b) A cross section of the asymmetric finger gate structure consisting of stripes of widths $d_1$ and $d_2$ and spacing $a_1$ and $a_2$ forming a superlattice with periodicity $d = d_1 + a_1 + d_2 + a_2$. (c) Sketch of the HgTe/(Hg,Cd)Te heterostructure under incident terahertz radiation indicating also the QW layer sequence.

of the Hall coefficient and identifies the charge neutrality point (CNP). For the investigated structures with 6.3, 7.0, and 8.0 nm QW thickness at zero gate voltage, the carrier concentrations are in the range of $(1.3–7.4) \times 10^{11}$ cm$^{-2}$, and mobilities are about $(5.0–8.5) \times 10^4$ cm$^2$ V$^{-1}$ s$^{-1}$.

To excite the ratchet effects, we apply normal-incident terahertz radiation of a continuous-wave optically pumped molecular laser; see Fig. 1(c). The laser is operated at a frequency $f = 2.54$ THz (wavelength $\lambda = 118$ $\mu$m, photon energy $\hbar\omega = 10.5$ meV). The samples are placed in an optical cryostat with $z$-cut quartz and poly(4-methyl-1-pentene), trade name TPX, windows. In order to block visible and near-infrared radiation, the windows are additionally covered with a black polyethylene film. The laser beam is focused using off-axis parabolic mirrors onto a spot with a diameter of about 1.5 mm, which is much larger than the area of the DGG structure. The radiation power $P$ during the measurements is monitored by a pyroelectric detector and in the sample position $P$ is about 20 mW. Accordingly, the radiation intensity $I$ at the sample is about 1 W cm$^{-2}$. More details on the system can be found in Refs. [16,17,35,36]. The radiation is modulated by a chopper with a frequency of 35 Hz and a standard lock-in technique is used to detect the photoresponse, measured as voltage drop $V_{\rm ph}$ across the sample resistance $R_{\rm S}$. All measurements are performed at helium temperature $T = 4.2$ K.

To explore the polarization dependence of the terahertz radiation-induced signal, we controllably vary the radiation Stokes parameters. The polarization is modified by placing a crystal quartz $\lambda/4$ plate in front of the sample, which is rotated by a phase angle $\varphi$ between the $c$ axis of the plate and the electric field vector of the laser radiation.

This allows us to vary the degree of circular polarization $P_{\rm circ} = \sin 2\varphi$, which corresponds to the Stokes parameter $s_3$, as well as the degrees of the linear polarization (these Stokes parameters are $s_1/s_0 = \sin 4\varphi/2$ and $s_2/s_0 = (1 + \cos 4\varphi)/2$) [37]). Additionally, we perform measurements in which the vector of the electric field **E** is rotated by a $\lambda/2$ plate. In this case, the azimuth angle $\alpha$ between **E** and the $x$ direction determines the orientation of the incident radiation regarding the gate stripes, see Fig. 1(c), and the Stokes parameters are described by $s_1/s_0 = \sin 2\alpha$ and $s_2/s_0 = \cos 2\alpha$ [37].

### B. Results

Figure 2 shows the dependence of the photosignal excited in sample D7 (QW thickness $d_{\rm QW} = 7$ nm) on the phase angle $\varphi$. The signal change $V_{\rm ph}$ when changing the polarization is characteristic for the ratchet effects and can be well described by the function [22,32]

$$V_{\rm ph}(\varphi) = V_0 + V_{\rm L1}\frac{\sin 4\varphi}{2} + V_{\rm L2}\frac{1 + \cos 4\varphi}{2} + V_{\rm circ}\sin 2\varphi,$$

(1)

where the fitting parameters $V_0$, $V_{\rm L1}$, $V_{\rm L2}$, and $V_{\rm circ}$ describe the polarization-independent ratchet contribution ($V_0$, also called Seebeck ratchet), the linear ratchet effect ($V_{\rm L1}$, $V_{\rm L2}$), and the circular ratchet effect ($V_{\rm circ}$), respectively. This characteristic polarization dependence is detected for all samples and gives a first hint that we are dealing with a ratchet effect. Note that the above equation reflects the linear combination of the radiation Stokes parameters $s_0, s_1, s_2$, and $s_3$ with different weights. For right- ($\sigma^+$) and left- ($\sigma^-$) handed circularly polarized radiation, the Stokes
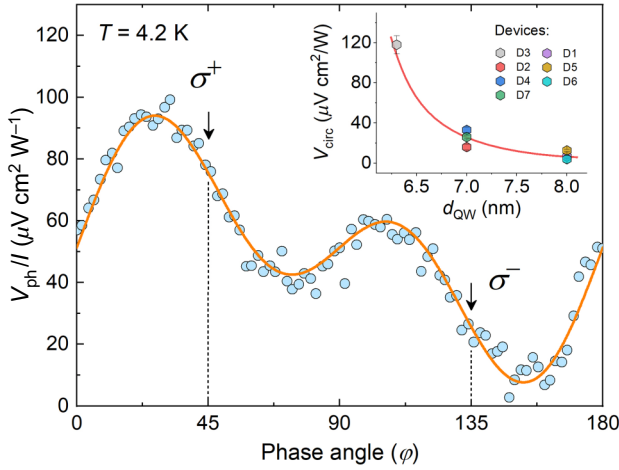
FIG. 2. Helicity dependence of the photovoltage of sample D7 normalized to the intensity under normally incident radiation with frequency $f = 2.54$ THz. Measurements are carried out at $T = 4.2$ K and zero gate voltages. Arrows correspond to right-handed ($\sigma^+$) and left-handed ($\sigma^-$) circular polarizations. The orange line is a fit according to Eq. (1). The inset indicates the circular photoresponse as a function of the QW thickness for different devices (D1–D7).

parameter $s_3$ changes its sign, whereas $s_1$ and $s_2$ vanish and the first polarization-independent term in Eq. (1) remains constant. Consequently, the circular photoresponse can be calculated as the odd part of the voltage signal with respect to the radiation helicity

$$V_{circ} = \frac{V^{\sigma^+} - V^{\sigma^-}}{2}, \qquad (2)$$

where $V^{\sigma^+}$ is the measured photosignal at right-handed circular polarization ($\varphi = 45°$), and $V^{\sigma^-}$ corresponds to the measured photosignal at left-handed circular polarization ($\varphi = 135°$). The inset in Fig. 2 compares the circular contributions for the studied devices having different quantum well thickness. One can see that the most pronounced feature of the ratchet effect is observed in device D3 ($d_{QW} = 6.3$ nm) with a quantum well thickness close to the critical one, i.e. hosting two-dimensional massless fermions.

For linearly polarized radiation, the last contribution in Eq. (1) vanishes and the polarization dependences of the second and third terms are given by $s_1/s_0 = \sin 2\alpha$ and $s_2/s_0 = \cos 2\alpha$ with amplitudes $V_{L1}$, and $V_{L2}$, respectively (not shown). To ensure that the detected signal is caused by the ratchet effects, we study the photoresponse as a function of the top gate voltages. According to theory [22], the ratchet contributions should reverse sign upon inversion of the lateral asymmetry parameter given by [22]

$$\Xi = \overline{|E(x)|^2 \frac{dV(x)}{dx}}. \qquad (3)$$

The overline means an average over the coordinate perpendicular to the DGG stripes. Here $V(x)$ is the electrostatic potential induced by the lateral superlattice, $E(x)$ is the spatially modulated near electric field of radiation acting on charge carriers in the QW. Consequently, it is controlled by the potential variation $dV(x)/dx$, which is determined by the voltages applied to the individual gates, $V_{G1}$ and $V_{G2}$. In order to tune the lateral asymmetry, we hold one of the gates at zero bias and vary the gate voltage on the other. Figure 3 demonstrates that the photosignals obtained upon variation of $V_{G1}$ and $V_{G2}$, i.e., by the interchange of gate voltage polarities at narrow and wide gates, have consistently opposite signs. This observation, exemplarily presented for the device D6 and left-handed circularly polarized radiation, agrees well with the signature of ratchet photovoltages, $V_{ph} \propto \Xi$, and proves that ratchet effects are responsible for the signal. Note that the dependencies are not exactly opposite to each other. This is explained both by the asymmetry caused by the built-in potential due to the metallic top gate stripes, and a somewhat different modulation of the carrier density in the QW upon applications of $V_{G1}$ and $V_{G2}$ (see inset in Fig. 3).

Strikingly, for high negative potentials applied to the top gates ($V_{G1}$ or $V_{G2}$), the photosignal exhibits sign-alternating oscillations when varying the top gate voltage. The number of oscillations in the ratchet photosignal depends on the QW thickness; see Fig. 4. The photosignal oscillations are detected for both linear and circular ratchet effects. Note that the sample resistance varies smoothly
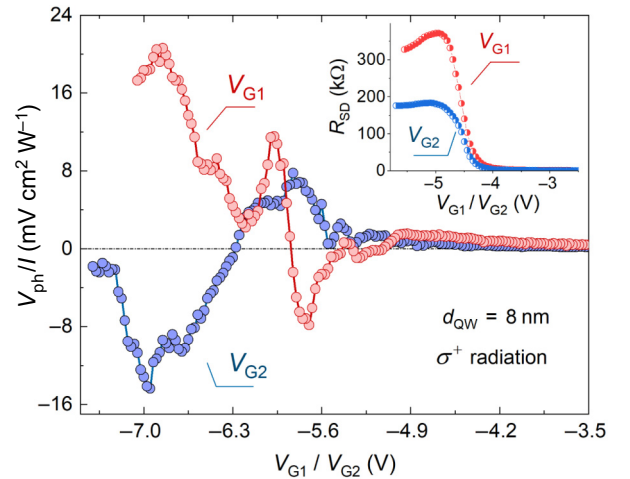


FIG. 3. Photovoltage normalized to the intensity as a function of the gate voltage for device D6. Red and blue lines correspond to gate voltages applied to electrodes with thin (G1) and thick (G2) fingers, respectively. Measurements are performed under normally incident right-handed circularly polarized radiation ($\sigma^+$) with frequency $f = 2.54$ THz and $T = 4.2$ K. The inset shows the resistance $R_{SD}$ vs gate voltage applied to thin stripes $V_{G1}$ ($V_{G2} = 0$, red symbols) and to thick stripes $V_{G2}$ ($V_{G1} = 0$, blue symbols).
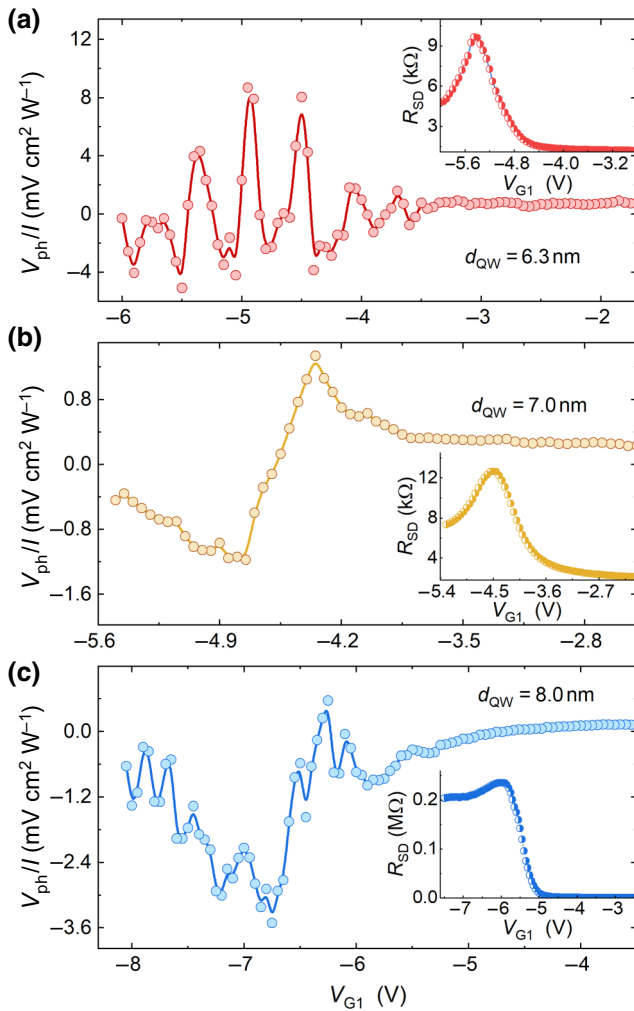
FIG. 4. (a)–(c) Photovoltage normalized to the intensity in devices D3, D2, and D5 versus gate voltage $V_{G1}$. All data are obtained at normal incidence of linearly polarized radiation with frequency $f = 2.54$ THz at $\alpha_{max}$, and $T = 4.2$ K. Here $\alpha_{max}$ is the azimuth angle at which the signal achieves its maximum. The solid lines are smoothed curves. Insets show results of transport measurements in HgTe QW devices D3, D2, and D5. The resistances are measured between source and drain as a function of the gate voltage $V_{G1}$.

with the gate voltage and only exhibits a peak at the CNP corresponding to the transition from $n$- to $p$-type conductivity; see insets in Fig. 4. We also emphasize that the oscillations appear for gate voltages corresponding to $p$-type conductivity.

The overall features of the observed terahertz photoresponse, in particular its proportionality to the lateral asymmetry parameter (see Fig. 3), clearly indicates that it is caused by the ratchet effect. Measurements on QWs with different thicknesses reveal that the magnitude of the ratchet effect in HgTe-based structures increases substantially (more than an order of magnitude) with decreasing quantum well width and becomes maximal for the QW

with critical thickness; see the inset in Fig. 2. This we ascribe to the qualitative change of the energy dispersion, which changes from parabolic with inverted band structure to a linear one for the critical thickness (6.4 nm).

The key result of the present work is the observation of the unexpected ratchet current oscillations when varying the top gate voltages; see Figs. 3 and 4. While the sample resistance shows the conventional behavior for narrow band HgTe systems with a resistance maximum at $V_{CNP}$ (see insets in Figs. 3 and 4), the ratchet responses in all samples exhibit sign-alternating oscillations for high negative top gate voltages. Furthermore, the amplitude of the ratchet effects drastically increases by more than two orders of magnitude, as compared with that detected for lower gate voltages at which the samples have $n$-type conductivity; see Figs. 3 and 4. While oscillations and increase of the ratchet current magnitude are detected in all samples, the number of oscillations is specific for each sample and is maximal for the quantum well structures with critical $d_{QW}$ in which the energy gap is very small or vanishing; see Fig. 4(a). Whereas giant oscillations have been detected in DGG structures in an external magnetic field [31,38–41], no oscillations in the ratchet voltage have been observed at zero magnetic field. In the next section we discuss the origin of these photocurrent oscillations in HgTe-based DGG structures, thus revealing peculiar features of the valence band energy spectrum in HgTe quantum wells with different QW thicknesses.

## II. DISCUSSION

To explore the origin of the observed oscillations, we develop a theory for ratchet currents in the HgTe quantum wells with $p$-type conductivity. To be specific, we consider the polarization-independent contribution of the photocurrent, which is generated via energy relaxation of the radiation-heated holes (the Seebeck ratchet). A detailed description of this mechanism can be found in Refs. [22,38]. The theory of polarization-dependent ratchet currents is out of the scope of the present manuscript. However, it can be developed using kinetic theory from [42,43] taking into account the complicated band structure of the QW.

The knowledge of the band structure is crucially needed for the theory of electric current generation and understanding of the oscillation origin. The energy dispersion of differently wide quantum wells, shown in Fig. 5, is calculated within the framework of an eight-band $\mathbf{k} \cdot \mathbf{p}$ model described in detail in Ref. [16]. The energy dispersion of the hole sub-bands varies greatly with the change of quantum well width. The 6.3-nm quantum well has a bandgap close to zero, for the 7-nm width, the band gap between hole and electrons is increased and, for the 8-nm-thick QW, bottom electron and top hole sub-bands are pushed even further away at the $\Gamma$ point; however, the
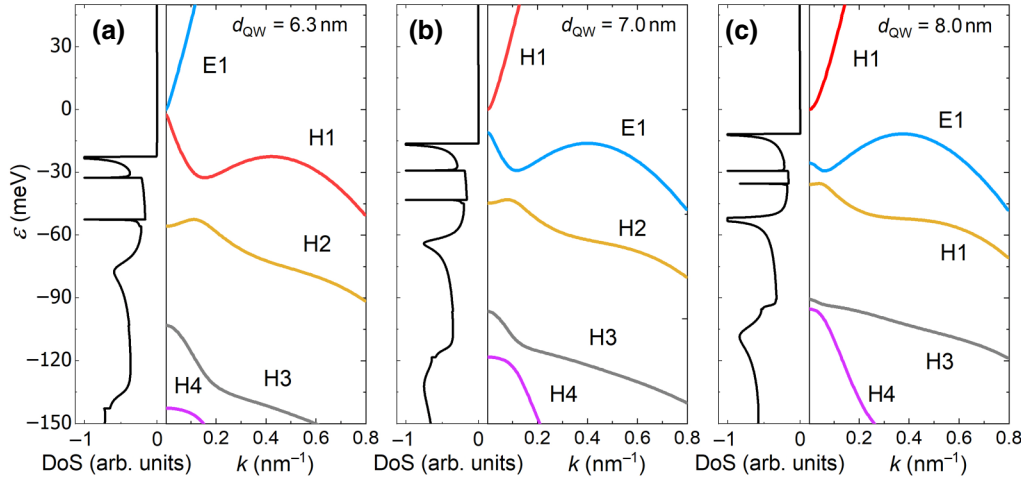
FIG. 5. The calculated energy spectra of the quantum wells of width 6.3 nm (a), 7 nm (b), and 8 nm (c) shown by colored lines. Black lines on the left side of the panels show the DOS for the corresponding energy spectra obtained in isotropic approximation.

quantum well has an indirect bandgap due to the anticrossing between first and second hole sub-bands. We consider the case of low temperatures, when free charge carriers are described by a nearly degenerate distribution function. In this case, the electronic properties are determined by carriers near the Fermi energy. For certain values, the Fermi level crosses the spectrum at several wave vector values, so that there are essentially multiple types of carriers, each with its own Fermi velocity and density, all of which contribute to both conductivity and ratchet current. Due to the anticrossing in the valence band, multiple Van Hove singularities are observed in the density of states (DOS). This is shown on the left-hand sides of Figs. 5(a)–5(c). Both momentum relaxation time and charge carrier density change significantly when the Fermi energy is close to these singularities. As will be shown below, these are the reasons for the drastic change of the ratchet current magnitude and direction.

Now we turn to the microscopic theory of the Seebeck ratchet current, which is based on models previously developed in Refs. [32,39]. The Seebeck ratchet current emerges when there is a phase difference between the in-plane component of the static electric field $\partial V(x)/\partial x$ caused by the electric potential induced by DGG and the spatially modulated free charge carrier heating caused by the electric near-field radiation. To calculate the ratchet current first, we split the time-independent part of the distribution function as $f_{\mathbf{p},\nu} = f_{\mathbf{p},\nu}^{+} + f_{\mathbf{p},\nu}^{-}$, where $\mathbf{p}$ is the charge carrier momentum, $\nu$ is the sub-band index, and $f_{\mathbf{p},\nu}^{+}$ and $f_{\mathbf{p},\nu}^{-}$ are even and odd on the momentum parts of the distribution function, respectively. The Boltzmann kinetic equation leads to the relation

$$-\frac{f_{\mathbf{p},\nu}^{-}}{\tau_p} = v_x \frac{\partial f_{\mathbf{p},\nu}^{+}}{\partial x} - \frac{\partial V}{\partial x}\frac{\partial f_{\mathbf{p},\nu}^{+}}{\partial p_x}, \quad (4)$$

where $\tau_p$ is the momentum relaxation time, $\mathbf{v}$ is the velocity defined as $\partial \varepsilon_{\mathbf{p},\nu}/\partial \mathbf{p}$, and $\varepsilon_{\mathbf{p},\nu}$ is the charge carrier energy.

The Seebeck ratchet current is obtained by summing over all momentum and sub-band indices $j_x = 2e \sum_{\mathbf{p},\nu} v_x f_{\mathbf{p},\nu}^{-}$, where the factor 2 stands for spin degeneracy. The ratchet current, which is linear in both $V(x)$ and radiation intensity, is given by

$$j_x = -\frac{1}{e}\sigma\frac{\partial V}{\partial x} - \frac{1}{e}\frac{\partial}{\partial x}S, \quad (5)$$

where conductivity $\sigma$ and $S$ are given by

$$\sigma = e^2 \sum_{\mathbf{p},\nu} v^2 \tau_p \left(-\frac{\partial f_{\mathbf{p},\nu}^{+}}{\partial \varepsilon_{\mathbf{p},\nu}}\right), \qquad S = e^2 \sum_{\mathbf{p},\nu} v^2 \tau_p f_{\mathbf{p},\nu}^{+}. \quad (6)$$

Due to fast electron-electron interaction, the electron gas is locally thermalized and $f_{\mathbf{p}}^{+}$ is described by the Fermi-Dirac distribution function

$$f_{\mathbf{p},\nu}^{+} = \left[\exp\left(\frac{\varepsilon_{\mathbf{p},\nu} + V(x) - \varepsilon_F - \delta\varepsilon_F(x)}{T + \delta T(x)}\right) + 1\right]^{-1}, \quad (7)$$

where $\delta T(x)$ and $\delta\varepsilon_F(x)$ are small nonequilibrium corrections of the temperature and Fermi energy induced by radiation. Since no current flows without radiation or at $V(x) = 0$, these conditions yield

$$\sigma_0 = \frac{\partial S_0}{\partial \varepsilon_F}, \qquad 0 = \frac{\partial S_0}{\partial \varepsilon_F}\frac{\partial \delta\varepsilon_F(x)}{\partial x} + \frac{\partial S_0}{\partial T}\frac{\partial \delta T(x)}{\partial x}, \quad (8)$$

where $\sigma_0$ and $S_0$ are values obtained from Eq. (6) at thermal equilibrium for $V(x) = 0$.

Equation (8) gives us an expression for the correction to the Fermi energy,

$$\delta\varepsilon_F = -\frac{\partial S_0/\partial T}{\sigma_0}\delta T + \delta\tilde{\varepsilon}. \quad (9)$$

Here, $\delta\tilde{\varepsilon}$ is a constant independent of $x$, which takes into account the fact that the radiation does not change the

average value of the carrier density. Spatial temperature oscillations can be found using the energy balance

$$|E(x)|^2 \frac{\sigma_0}{1 + \omega^2 \tau_p^2} = \frac{\delta T(x)}{\tau_T},$$

where $\tau_T$ is the temperature relaxation time. Finally, using the relation for the equilibrium distribution function $\partial f_{\mathbf{p},\nu}^{(0)}/\partial T = (\partial f_{\mathbf{p},\nu}^{(0)}/\partial \varepsilon_{\mathbf{p},\nu})(\varepsilon_{\mathbf{p},\nu} - \varepsilon_F)/T$ we obtain the Seebeck ratchet current

$$j_x = -\frac{1}{e} \frac{\sigma_0 \tau_T}{1 + \omega^2 \tau_p^2} \left( \frac{\partial \sigma_0}{\partial T} - \frac{\pi^2}{6} T \left( \frac{\partial \sigma_0}{\partial \varepsilon_F} \right)^2 \frac{1}{\sigma_0} \right) \overline{|E(x)|^2 \frac{\partial V}{\partial x}}.$$

(10)

To estimate the photocurrent, we make some simplifications: we assume that the momentum relaxation rate is proportional to the number of states where charge carriers can scatter. Similar assumptions can be made about $\tau_T$, so that both $\tau_T^{-1}$, $\tau_p^{-1} \propto g(\varepsilon_{\mathbf{p},\nu})$, where $g(\varepsilon_{p,\nu})$ is the density of states. We also ignore the anisotropy of the charge carriers spectrum in HgTe quantum wells and take into account only its isotropic part. Figure 6 shows the dependencies of the ratchet current for different quantum wells at $T = 4.2$ K. It is clearly seen that the ratchet current is highly sensitive to the details of the energy spectrum. A complex structure is observed in the dependence of the ratchet current on the Fermi energy, which follows the DOS. When the Fermi energy is close to regions of a high gradient of the density of states or one of the Van Hove singularities, the Seebeck ratchet current is drastically increased or changes its direction; see the vertical dashed lines in Fig. 6. The latter is caused by the large value of the derivative of the conductivity with respect to the Fermi energy and temperature for these energies; see Eq. (10). By contrast, in regions where the Fermi energy is far from any features of the DOS, the photocurrent is several orders of magnitude lower. Note that the complicated band structure of HgTe quantum wells does not allow us to convert the $\varepsilon_F$ scale to the $V_G$ scale.

The developed theoretical model provides evidence that ratchet current oscillations arise due to Van Hove singularities and/or abrupt changes in the DOS. In fact, for corresponding values of $\varepsilon_F$, the derivatives of the conductivity with respect to the Fermi energy and temperature are large and, according to Eq. (10), the photocurrent reaches its maximum. As can be seen on the left sides of Figs. 5(a)–5(c), regions of a high gradient of the density of states and the Van Hove singularities are located in the range of negative $\varepsilon_F$. By contrast, at positive $\varepsilon_F$ the energy dependencies of the DOS are weak, and derivatives $\partial \sigma_0/\partial \varepsilon_F$ and $\partial \sigma_0/\partial T$ are much smaller. Thus, ratchet currents in $p$-type conducting QWs are much higher than in $n$-type conducting QWs.
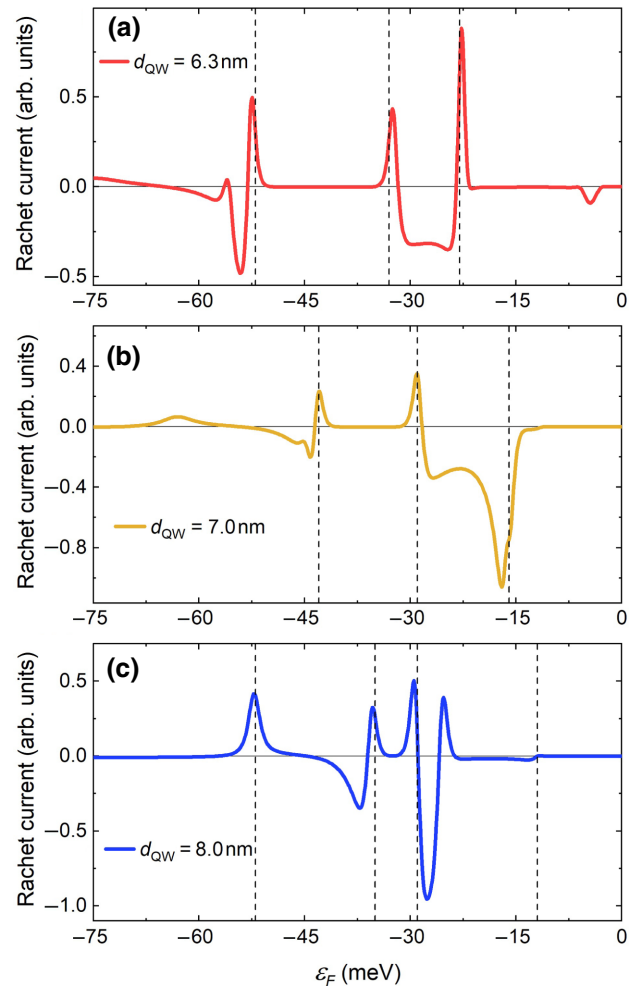


FIG. 6. Dependencies of the Seebeck ratchet current on the Fermi energy for HgTe quantum wells of different widths. Photocurrents are calculated after Eq. (10) using DOS and electron energy spectra from Fig. 5. The vertical dashed lines correspond to the Van Hove singularities in the DOS.

The developed theory describes well the main features of the experimental results. Indeed, the theoretical model shows the occurrence of (i) singularities, (ii) sign changes of the photocurrent for different gate voltages (and consequently Fermi energies) in rough agreement to those observed in the experiments (see Figs. 3, 4, and 6), and (iii) that the amplitude of the photocurrent oscillations is much higher in structures with $p$-type QWs, in which singularities are possible. Therefore, we want to emphasize that despite several simplifications, the presented model provides evidence of the main responsible physical phenomena. Quantitative comparisons, however, require several model refinements. First, the electrostatic problem for the structure should be solved to calculate the Fermi energy and potential $V(x)$ dependence on the two gate voltages applied to the DGG. Second, $\tau_p$, $\tau_T$ should be accurately calculated for different wave vectors and band

indices both for scattering by impurities and phonons taking into account the spectrum anisotropy and the fact that the wave function of carriers in the QW has contributions from the $\Gamma_7$, $\Gamma_8$, and $\Gamma_6$ bands each with its own envelope functions along the $z$ axis. The accurate treatment of relaxation times will significantly alter the ratchet current dependencies shown in Fig. 6. Lastly, when the Fermi energy exactly matches the energy of one of the Van Hove singularities, the theory loses its applicability, since the difference between electron kinetic energy and local extreme in the energy spectrum goes to zero, and $V(x)$ cannot be considered small. As a result, the ratchet current should be expressed in all orders of $V(x)$. These more precise results can be obtained numerically, but they will not bring new and/or deeper physical understanding.

Finally, we comment on the dependence of the circular photoresponse on the QW thickness. The data presented in the inset in Fig. 2 indicate that the ratchet current increases with a decrease of the QW thickness from 8.0 to 6.3 nm. The trend is opposite to that expected for the circular photogalvanic effect (CPGE) in nonstructured HgTe-based QW structures: according to the results of a theoretical analysis the CPGE current increases monotonically for an increase of the HgTe QW thickness from 5 to 9 nm [44]. However, it should be noted that the mechanism of the circular ratchet current (for a review, see Ref. [22]) is completely different from that of the CPGE in nonstructured QWs. It requires a periodic structure that causes two kinds of asymmetric lateral modulations: (i) of the electrostatic potential $V$ and (ii) of the terahertz wave amplitude $E$. These microscopic mechanisms can be characterized by different dependences on the QW width. As a first indication of the different behavior of CPGE and the ratchet current, we can recall the fact that, according to the results of Ref. [44], the linear photogalvanic effect is expected to be negligible compared with the CPGE, whereas in our experiments on the ratchet effect, linear and circular ratchet currents have almost the same magnitude. A detailed theoretical study of the thickness dependence is out of the scope of the present paper.

## III. CONCLUSIONS

To summarize, different kinds of terahertz ratchet effects, including the circular, linear, and polarization-independent ratchets, are observed in HgTe-based DGG structures. In comparison with common semiconductors, HgTe QW structures exhibit unconventional band-structure properties, correlated to the quantum well thickness. Measurements on devices with different QW widths demonstrate that the magnitude of the circular ratchet effect increases for reduction of the QW width and is maximal in structures with critical QW thickness where the energy gap is close to zero. A further drastic increase of the ratchet current magnitude is obtained by applying high

negative top gate voltages resulting in $p$-type conductivity beneath the gates. The enhancement of the photoresponse as well as the observed sign-alternating oscillations with gate voltage are shown to be caused by the complex valence band structure of HgTe-based QWs. Our study of ratchet currents in HgTe DGG devices paves the way to develop terahertz detectors with substantially increased responsivity and opens up access to the analysis of energy dispersion details, including the properties of the valence band.

[1] P. Capper, *Narrow-Gap II-VI Compounds for Optoelectronic and Electromagnetic Applications* (Springer US, New York City, 1997).

[2] P. Norton, HgCdTe infrared detectors, Opto-Electron. Rev. **10**, 159 (2002).

[3] M. Henini and M. Razeghi, *Handbook of Infra-Red Detection Technologies* (Elsevier Science, Amsterdam, 2002).

[4] A. Rogalski, HgCdTe infrared detector material: History, status and outlook, Rep. Prog. Phys. **68**, 2267 (2005).

[5] S. A. Dvoretsky, N. N. Mikhailov, Y. G. Sidorov, V. A. Shvets, S. N. Danilov, B. Wittman, and S. D. Ganichev, Growth of HgTe quantum wells for IR to THz detectors, J. Electron. Mater. **39**, 918 (2010).

[6] C. Downs and T. E. Vandervelde, Progress in infrared photodetectors since 2000, Sensors **13**, 5054 (2013).

[7] A. Rogalski, *Infrared and Terahertz Detectors* (Taylor & Francis Ltd, Abingdon, 2018), 3rd ed.

[8] N. Vanamala, K. C. Santiago, and N. C. Das, Enhanced MWIR absorption of HgCdTe (MCT) via plasmonic metal oxide nanostructures, AIP Adv. **9**, 025113 (2019).

[9] H. Xu, J. Zhou, H. Wang, and J. Li, Giant photonic response of mexican-hat topological semiconductors for mid-infrared to terahertz applications, J. Phys. Chem. Lett. **11**, 6119 (2020).

[10] J. E. Moore and J. Orenstein, Confinement-Induced Berry Phase and Helicity-Dependent Photocurrents, Phys. Rev. Lett. **105**, 026805 (2010).

[11] M. Z. Hasan and C. L. Kane, Colloquium: Topological insulators, Rev. Mod. Phys. **82,** 3045 (2010).

[12] J. Zhang, C.-Z. Chang, Z. Zhang, J. Wen, X. Feng, K. Li, M. Liu, K. He, L. Wang, X. Chen, Q.-K. Xue, X. Ma, and Y. Wang, Band structure engineering in $(Bi_{1-x}Sb_x)_2Te_3$ ternary topological insulators, Nat. Commun. **2,** 574 (2011).

[13] C. R. Becker, X. C. Zhang, A. Pfeuffer-Jeschke, K. Ortner, V. Hock, G. Landwehr, and L. W. Molenkamp, Very large Rashba spin–orbit splitting in HgTe quantum wells, J. Supercond. **16,** 625 (2003).

[14] M. König, S. Wiedmann, C. Brüne, A. Roth, H. Buhmann, L. W. Molenkamp, X.-L. Qi, and S.-C. Zhang, Quantum spin hall insulator state in HgTe quantum wells, Science **318,** 766 (2007).

[15] A. Roth, C. Brüne, H. Buhmann, L. W. Molenkamp, J. Maciejko, X.-L. Qi, and S.-C. Zhang, Nonlocal transport in the quantum spin hall state, Science **325,** 294 (2009).

[16] K.-M. Dantscher, D. A. Kozlov, P. Olbrich, C. Zoth, P. Faltermeier, M. Lindner, G. V. Budkin, S. A. Tarasenko, V. V. Bel'kov, Z. D. Kvon, N. N. Mikhailov, S. A. Dvoretsky, D. Weiss, B. Jenichen, and S. D. Ganichev, Cyclotron-resonance-assisted photocurrents in surface states of a three-dimensional topological insulator based on a strained high-mobility HgTe film, Phys. Rev. B **92,** 165314 (2015).

[17] K.-M. Dantscher, D. A. Kozlov, M. T. Scherr, S. Gebert, J. Bärenfänger, M. V. Durnev, S. A. Tarasenko, V. V. Bel'kov, N. N. Mikhailov, S. A. Dvoretsky, Z. D. Kvon, J. Ziegler, D. Weiss, and S. D. Ganichev, Photogalvanic probing of helical edge channels in 2D HgTe topological insulators, Phys. Rev. B **95,** 201103(R) (2017).

[18] B. Wittmann, S. N. Danilov, V. V. Bel'kov, S. A. Tarasenko, E. G. Novik, H. Buhmann, C. Brüne, L. W. Molenkamp, Z. D. Kvon, N. N. Mikhailov, S. A. Dvoretsky, N. Q. Vinh, A. F. G. van der Meer, B. Murdin, and S. D. Ganichev, Circular photogalvanic effect in HgTe/HgCdTe quantum well structures, Semicond. Sci. Technol. **25,** 095005 (2010).

[19] S. N. Danilov, B. Wittmann, P. Olbrich, W. Eder, W. Prettl, L. E. Golub, E. V. Beregulin, Z. D. Kvon, N. N. Mikhailov, S. A. Dvoretsky, V. A. Shalygin, N. Q. Vinh, A. F. G. van der Meer, B. Murdin, and S. D. Ganichev, Fast detector of the ellipticity of infrared and terahertz radiation based on HgTe quantum well structures, J. Appl. Phys. **105,** 013106 (2009).

[20] P. Olbrich, J. Allerdings, V. V. Bel'kov, S. A. Tarasenko, D. Schuh, W. Wegscheider, T. Korn, C. Schüller, D. Weiss, and S. D. Ganichev, Magnetogyrotropic photogalvanic effect and spin dephasing in (110)-grown $GaAs/Al_xGa_{1-x}As$ quantum well structures, Phys. Rev. B **79,** 245329 (2009).

[21] P. Olbrich, J. Karch, E. L. Ivchenko, J. Kamann, B. März, M. Fehrenbacher, D. Weiss, and S. D. Ganichev, Classical ratchet effects in heterostructures with a lateral periodic potential, Phys. Rev. B **83,** 165320 (2011).

[22] E. L. Ivchenko and S. D. Ganichev, Ratchet effects in quantum wells with a lateral superlattice, JETP Lett. **93,** 673 (2011)., [Pisma v ZhETF **93,** 752 (2011)]

[23] V. V. Popov, D. V. Fateev, T. Otsuji, Y. M. Meziani, D. Coquillat, and W. Knap, Plasmonic terahertz detection by a double-grating-gate field-effect transistor structure with an asymmetric unit cell, Appl. Phys. Lett. **99,** 243504 (2011).

[24] E. S. Kannan, I. Bisotto, J.-C. Portal, R. Murali, and T. J. Beck, Photovoltage induced by ratchet effect in Si/SiGe heterostructures under microwave irradiation, Appl. Phys. Lett. **98,** 193505 (2011).

[25] T. Otsuji, T. Watanabe, S. A. B. Tombet, A. Satou, W. M. Knap, V. V. Popov, M. Ryzhii, and V. Ryzhii, Emission and detection of terahertz radiation using two-dimensional electrons in III–V semiconductors and graphene, IEEE Trans. Terahertz Sci. Technol. **3,** 63 (2013).

[26] S. Boubanga-Tombet, Y. Tanimoto, A. Satou, T. Suemitsu, Y. Wang, H. Minamide, H. Ito, D. V. Fateev, V. V. Popov, and T. Otsuji, Current-driven detection of terahertz radiation using a dual-grating-gate plasmonic detector, Appl. Phys. Lett. **104,** 262104 (2014).

[27] P. Faltermeier, P. Olbrich, W. Probst, L. Schell, T. Watanabe, S. A. Boubanga-Tombet, T. Otsuji, and S. D. Ganichev, Helicity sensitive terahertz radiation detection by dual-grating-gate high electron mobility transistors, J. Appl. Phys. **118,** 084301 (2015).

[28] G. Rupper, S. Rudin, and M. S. Shur, Ratchet Effect in Partially Gated Multifinger Field-Effect Transistors, Phys. Rev. Appl. **9,** 064007 (2018).

[29] A. Yu, Plasmon ratchet effect with electrons and holes simultaneously existing in the graphene channel: A promising effect for the terahertz detection, J. Phys. D: Appl. Phys. **51,** 395103 (2018).

[30] J. A. Delgado-Notario, V. Clericò, E. Diez, J. E. Velázquez-Pérez, T. Taniguchi, K. Watanabe, T. Otsuji, and Y. M. Meziani, Asymmetric dual-grating gates graphene FET for detection of terahertz radiations, APL Photonics **5,** 066102 (2020).

[31] P. Sai, S. O. Potashin, M. Szoła, D. Yavorskiy, G. Cywiński, P. Prystawko, J. Łusakowski, S. D. Ganichev, S. Rumyantsev, W. Knap, and V. Y. Kachorovskii, Beatings of ratchet current magneto-oscillations in GaN-based grating gate structures: Manifestation of spin-orbit band splitting, Phys. Rev. B **104,** 045301 (2021).

[32] P. Olbrich, J. Kamann, M. König, J. Munzert, L. Tutsch, J. Eroms, D. Weiss, M.-H. Liu, L. E. Golub, E. L. Ivchenko, V. V. Popov, D. V. Fateev, K. V. Mashinsky, F. Fromm, T. Seyller, and S. D. Ganichev, Terahertz ratchet effects in graphene with a lateral superlattice, Phys. Rev. B **93,** 075422 (2016).

[33] M. Majewicz, D. Śnieżek, T. Wojciechowski, E. Baran, P. Nowicki, T. Wojtowicz, and J. Wróbel, Low temperature processing of nanostructures based on II-VI semiconductors quantum wells, Acta Phys. Pol., A **126,** 00 (2014).

[34] M. M. Majewicz, *Wytwarzanie nanostruktur i badanie zjawisk transportu w dwuwymiarowych izolatorach topologicznych* (PhD thesis, Institute of Physics PAS, Warsaw, 2019).

[35] V. A. Shalygin, H. Diehl, C. Hoffmann, S. N. Danilov, T. Herrle, S. A. Tarasenko, D. Schuh, C. Gerl, W. Wegscheider, W. Prettl, and S. D. Ganichev, Spin photocurrents and the circular photon drag effect in (110)-grown quantum well structures, JETP Lett. **84,** 570 (2007).

[36] H. Plank, L. E. Golub, S. Bauer, V. V. Bel'kov, T. Herrmann, P. Olbrich, M. Eschbach, L. Plucinski, C. M. Schneider, J. Kampmeier, M. Lanius, G. Mussler, D. Grützmacher, and S. D. Ganichev, Photon drag effect in

$(Bi_{1-x}Sb_x)_2Te_3$ three-dimensional topological insulators, Phys. Rev. B **93**, 125434 (2016).

[37] V. V. Bel'kov, S. D. Ganichev, E. L. Ivchenko, S. A. Tarasenko, W. Weber, S. Giglberger, M. Olteanu, H. P. Tranitz, S. N. Danilov, P. Schneider, W. Wegscheider, D. Weiss, and W. Prettl, Magneto-gyrotropic photogalvanic effects in semiconductor quantum wells, J. Phys. Condens. Matter **17**, 3405 (2005).

[38] P. Faltermeier, G. V. Budkin, J. Unverzagt, S. Hubmann, A. Pfaller, V. V. Bel'kov, L. E. Golub, E. L. Ivchenko, Z. Adamus, G. Karczewski, T. Wojtowicz, V. V. Popov, D. V. Fateev, D. A. Kozlov, D. Weiss, and S. D. Ganichev, Magnetic quantum ratchet effect in (Cd, Mn)Te- and CdTe-based quantum well structures with a lateral asymmetric superlattice, Phys. Rev. B **95**, 155442 (2017).

[39] G. V. Budkin, L. E. Golub, E. L. Ivchenko, and S. D. Ganichev, Magnetic ratchet effects in a two-dimensional electron gas, JETP Lett. **104**, 649 (2016).

[40] P. Faltermeier, G. V. Budkin, S. Hubmann, V. V. Bel'kov, L. E. Golub, E. L. Ivchenko, Z. Adamus, G. Karczewski, T. Wojtowicz, D. A. Kozlov, D. Weiss, and S. D. Ganichev, Circular and linear magnetic quantum ratchet effects in dual-grating-gate CdTe-based nanostructures, Phys. E **101**, 178 (2018).

[41] S. Hubmann, V. V. Bel'kov, L. E. Golub, V. Y. Kachorovskii, M. Drienovsky, J. Eroms, D. Weiss, and S. D. Ganichev, Giant ratchet magneto-photocurrent in graphene lateral superlattices, Phys. Rev. Res. **2**, 033186 (2020).

[42] M. V. Durnev, Photovoltaic hall effect in the two-dimensional electron gas: Kinetic theory, Phys. Rev. B **104**, 085306 (2021).

[43] A. V. Nalitov, L. E. Golub, and E. L. Ivchenko, Ratchet effects in two-dimensional systems with a lateral periodic potential, Phys. Rev. B **86**, 115301 (2012).

[44] J. Li, W. Yang, J.-T. Liu, W. Huang, C. Li, and S.-Y. Chen, Enhanced circular photogalvanic effect in HgTe quantum wells in the heavily inverted regime, Phys. Rev. B **95**, 035308 (2017).